NJC

ROYAL SOCIETY OF CHEMISTRY

PAPER

View Article Online
View Journal | View Issue

Cite this: *New J. Chem.*, 2025, **49**, 9475

Nanocellulose from coconut midrib used for antibacterial and electromagnetic interference shielding applications†

Joshua Jose and Vinod T. P. *

Midrib of coconut (*Cocos nucifera*) is a natural source of cellulose, which is renewable and biodegradable. The use of natural cellulose for practical applications exemplifies a sustainable reuse of agricultural waste. This work presents the preparation of nanocellulose from coconut midrib using optimized pretreatment and acid hydrolysis processes. The resulting nanocellulose was characterized through various analyses to confirm the morphology and composition. Nanocellulose thus synthesized was used for preparing cellulose nanopaper. In order to improve the water resistance of the cellulose nanopaper, we used a simple approach of functionalization by impregnating it with chitosan (CS), followed by *in situ* polymerization of polypyrrole (PPy) in the matrix. The functionalized cellulose nanopaper shows good electrical conductivity and an electromagnetic interference (EMI) shielding effectiveness of 21.92 dB at 10 GHz, which makes it a potential material for EMI shielding applications. In addition, the functionalized cellulose nanopaper exhibits bacterial reductions of 93.47% and 82.79% towards *Staphylococcus aureus* and *Escherichia coli*, respectively. This work provides a facile and efficient method for the synthesis of nanocellulose from coconut midrib and a useful approach to functionalize cellulose nanopaper. Cellulose nanopapers thus prepared were demonstrated to have applications in EMI shielding and antibacterial coating.

Received 6th March 2025,
Accepted 5th May 2025

DOI: 10.1039/d5nj01022e

rsc.li/njc

1. Introduction

The United Nations introduced sustainable development goals (SDGs), in 2015, to address various social, economic and environmental concerns of the member nations.[1] The accumulation of waste products and their management are major concerns in large scale industries and farming.[2] The attainment of the SDGs is dependent on proper disposal and upgrading of by-products/waste products from industry and farming. Inefficient waste disposal and waste management will impede the sustainable growth of society.[3] The by-products from the farming sector, especially from agriculture, are often dumped as waste and end up as a liability to farmers and to the environment/ecosystem. Efficient biomass management strategies are necessary in agriculture and farming as they not only offer a secondary income but also contribute to food safety.[4]

Coconut (*Cocos nucifera*) is one of the most abundantly cultivated crops in over 100 countries, and the production of coconut is estimated to be above 50 million tons per annum globally.[5] Coconut cultivation farms contribute to a high amount of biomass waste in the form of coconut husk, shell, frond, fiber, and midrib.[6] A small portion of this biomass is usually disposed of in the farms themselves as biofertilizers and also converted to value added products. But the amount of biomass recycled is much less compared to the total amount of coconut biomass produced.[7] The midrib of coconut is normally discarded in farms, and the decomposition time for midrib is higher than that for the other biomass produced in coconut cultivation.[8] The comparison of the cellulose, hemicellulose and lignin contents of coconut palm reveals an interesting composition. The midrib has the highest percentage of cellulose among the other parts of coconut palm, and also the lignin content of midrib is relatively less.[9] The lower amount of lignin content makes the isolation of the cellulose from midrib easy, and it positively impacts the quality of the cellulose prepared. Cellulose is made up of D-glucopyranose rings linked by a 1,4-glycosidic bond.[10] Glucose residues, which are the repeating units of cellulose, contain one primary hydroxyl group and two secondary hydroxyl groups. These hydroxyl groups are the reason for the characteristic properties of cellulose.

Chitosan is a renewable polysaccharide derived from chitin shells of shrimps and crabs.[11] Chitosan can form a hydrogen bond with cellulose due to the presence of surface hydroxyl and amino groups.[12] The tensile strength and the water-resistant properties of cellulose nanopaper can be significantly increased by the addition of chitosan to it.[13] Also, the addition of chitosan

Department of Chemistry, CHRIST University, Bengaluru, 560029, India.
E-mail: vinod.tp@christuniversity.in

† Electronic supplementary information (ESI) available. See DOI: https://doi.org/10.1039/d5nj01022e

positively influences the antimicrobial properties of cellulose nanopaper.[14] Polypyrrole is a conducting polymer with potential applications in biomedical implants, EMI shielding, energy storage devices, flexible electronics and so forth.[15] The advantages of polypyrrole include low cost, ease of synthesis, biocompatibility and electrical conductivity.[16] The poor solubility in solvents along with inability to be used in direct melt processing hinders the use of polypyrrole-based structures for practical applications.[17] Researchers have shown that chitosan and polypyrrole composites can be used for anticorrosion coatings and biosensors due to the synergistic effects of chitosan and polypyrrole. The ease of polymerization and hydrophobic and conductive nature of polypyrrole along with its interaction with chitosan are used in composites to enhance the water resistance and conductive properties.[18,19]

In this work, we present nanocellulose synthesized from coconut midrib. To the best of our knowledge, this is the first report on the synthesis of nanocellulose from coconut midrib. The structural features, properties, and applications of these materials show marked differences in comparison with similar nanomaterials prepared from other parts of the coconut tree.[20–22] A composite film of nanocellulose with chitosan and polypyrrole was also prepared. The addition of chitosan and polypyrrole enhanced the physical properties of the nanocellulose film. Antibacterial studies of the nanocellulose film showed positive results. Electromagnetic interference (EMI) shielding studies were carried out, and the results show that the composite film is a successful candidate for practical use in EMI shielding.

2. Experimental section

2.1 Materials

Coconut leaves were collected from Hullahalli village, Karnataka, India, and leaflet midrib was peeled from the leaf. Sodium hydroxide (NaOH), hydrogen peroxide (H_2O_2), chitosan (CS) with a deacetylation degree of 85%, and sulphuric acid (H_2SO_4) were procured from Sigma Aldrich. Ammonium persulphate (APS), pyrrole and acetic acid were purchased from Nice Chemicals and were used without further purification.

2.2 Synthesis of coconut palm leaflet midrib nanocellulose

2.2.1. Pretreatment of coconut midrib (CM) cellulose. The cellulose from coconut midrib was synthesized using a process which is a modification of the method reported by Faria *et al.*[23] The midrib was first cleaned, thoroughly washed with water, and then dried in sunlight for two days. Afterward, it was ground into a powder form and dried. 5 grams of the powder were weighed and added to 100 mL of 5% (w/v) sodium hydroxide solution. The mixture was then magnetically stirred for one hour at 75 °C. The reaction mixture was washed with water until neutral pH was reached. It was then washed and dried. This step is crucial in the delignification process of the fiber, as it determines the color of the resulting cellulose. The delignified fibers were added to 100 mL of a solution containing 4% sodium hydroxide (w/w) and 24% hydrogen peroxide (v/v) in a 1 : 1 ratio, and the mixture was stirred vigorously for two hours. The resulting mixture was then washed and sun dried to obtain the coconut midrib cellulose.

2.2.2. Preparation of nanocellulose. Nanocellulose was prepared by the acid hydrolysis of coconut midrib. This process was performed using 40% (w/w) sulfuric acid.[24] Approximately 5 grams of coconut midrib cellulose were weighed and added to 100 mL of sulfuric acid. The mixture was then stirred at room temperature for three hours. The reaction was stopped by adding distilled water to the solution. The mixture was stirred magnetically for two minutes. Following this, it was centrifuged for three cycles at 9000 rpm, with each cycle lasting 15 minutes. Following centrifugation, the acidic supernatant was removed and replaced with distilled water. The solution was then dialyzed with water to remove acid residues. Dialysis was carried out until the solution was neutralized. The coconut midrib nanocellulose collected from the membrane was vigorously stirred for 10 minutes to break down the particles. The nanocellulose sample was then collected and used for characterization.

2.3 Preparation of coconut midrib cellulose nanopaper

Coconut midrib nanopaper (CN) samples were prepared by adapting a method reported by Haishun Du *et al.*[25] 50 mL of a 1.0 wt% coconut midrib nanocellulose suspension was added to 200 mL of deionized water. This solution was then magnetically stirred for 2 hours and subsequently ultrasonicated for 10 minutes. The mixture was then transferred to a filtration setup, and filtration resulted in the formation of a film. The resulting film was covered with filter paper on both sides and dried on a hot plate for 2 hours. The nanocellulose film was subsequently kept under ambient conditions for further analysis.

2.3.1. Impregnation of coconut midrib cellulose nanopaper with chitosan (CS). A 1.5 wt% chitosan solution was prepared by dissolving chitosan in a 2% (v/v) aqueous acetic acid solution. The cellulose midrib nanopaper was soaked in freshly prepared chitosan solution and left for one hour at room temperature. The chitosan-impregnated CN was kept on a glass plate for 12 hours at room temperature to dry. The dried CN/CS samples were soaked in a 0.01 mol L^{-1} NaOH solution for one hour at room temperature to neutralize any remaining acetic acid. The resulting CN/CS samples were rinsed with distilled water and then dried.

2.3.2. Polymerization of polypyrrole (PPy) in the CN/CS films. A pyrrole monomer (0.5 mL, 7.21 mmol) was added to 25 mL of deionized water and stirred at room temperature for 30 minutes. The CN/CS film was then immersed in the pyrrole monomer solution in a Petri dish for one hour to allow the film to swell, which allows the absorption of the pyrrole monomer. Then, 10 mL of APS aqueous solution, of about 5.8 wt%, was added to the dish to start the polymerization process. After adding APS, the solution was left for one hour at room temperature. The CN/CS/PPy samples formed were rinsed with water to remove any surface residues. CN/PPy (without chitosan) was also prepared for comparison, from pure CN using the same process.[26]

2.4 Characterization

Fourier Transform Infrared (FTIR) spectra with a frequency range of 4000 to 500 cm^{-1} and a spectral resolution of 4 cm^{-1}

were obtained from the samples using a PerkinElmer Spectrum 100 spectrometer. A Bruker D Advance X-ray diffractometer was used to perform the X-ray diffraction investigation using Cu-Kα radiation with a wavelength of 1.5406 Å. The operating conditions of the diffractometer were set at 40 kV and 20 mA, and data were collected with the range of 10 to 90 degrees. The SEM images were obtained utilizing the Thermo Fisher Scientific, Apreo 2S, with a maximum accelerating voltage of 30 kV. HRTEM images were acquired using a JEOL JEM-2100, LaB6, operating at 200 kV. The suspension's particle size distribution was measured by dynamic light scattering (DLS) with a Zetasizer (ZS90) instrument. The atomic force microscopy (AFM) analysis was performed using a Bruker Innova, ICMS instrument. The current–voltage measurements were performed using an Ossila BV T2001A Four-Point Probe System.

2.5 Wettability and water uptake

The water contact angle was measured using Image-J software. The water contact angle measurements were taken immediately upon placing the water droplets onto the surface of the films. Each sample was measured three times at different locations, and the mean and standard deviations were estimated. The samples were initially cut into 0.5 cm × 0.5 cm strips in order to calculate the water uptake ratio. To eliminate any remaining moisture, the samples were subsequently stored for 24 hours at 70 °C in a vacuum oven. After that, the strips were submerged in DI water for half an hour. The initial weight of the samples was recorded as M_0 before immersion. After removal from the water, the weight of the film was recorded as M_1. The difference in weight before and after immersion determined the water uptake ratio, which is given by

$$\text{Water uptake ratio} = (M_1 - M_0)/M_0.$$

2.6 Antibacterial studies

To investigate the antibacterial properties, the four samples (CN, CN/CS, CN/PPy, and CN/CS/PPy) were tested against Gram-positive *Staphylococcus aureus* bacteria and Gram-negative *E. coli* bacteria. Using a sterile saline solution, the culture was diluted to around 5×10^5 CFU mL^{-1}. It was then centrifuged twice with Butterfield's phosphate buffer and re-suspended in the same buffer. The samples were divided into pieces with a radius of 1 cm before the antibacterial test. Two of these fragments were then put on a sterile plate. To ensure complete contact with the inoculated bacteria, 20 μL of the inoculum was then applied to the center of one specimen, and the second specimen was positioned on top. After the vortexing process, the liquid portion from each sample was subjected to a series of 10-fold serial dilutions. Each diluted sample was carefully plated on separate nutrient agar plates. These plates were then placed in an incubator set to 37 °C, where they rested for 24 hours. Once the time had passed, the bacterial colonies were counted and documented, paving the way for an analysis of the antimicrobial effectiveness of the treatment.

2.7 EMI shielding measurements

The EMI shielding performance of the samples was measured using a vector network analyser using the waveguide method in the frequency range of 8 to 12 GHz (X band). According to Schelkunoff theory, the total EMI effectiveness is the sum of microwave absorption (SE_A), microwave reflection (SE_R) and microwave multiple reflection (SE_M) of the electromagnetic wave when it interacts with the shielding object.[27] Microwave absorption (SE_A), microwave reflection (SE_R) and microwave multiple reflection (SE_M) can be calculated from the experimentally measured scattering parameters denoted as S_{11}, S_{12}, S_{22} and S_{21}. SE_M is negligible when SE_T is greater than 10 dB and can be omitted from the calculation. The total shielding effectiveness is the sum of the shielding effectiveness due to absorption, reflection and multiple reflections.[28] This can be obtained using the following equation:

$$SE_T = SE_A + SE_R + SE_M.$$

3. Results and discussion

3.1 Synthesis of coconut midrib nanocellulose

The coconut midrib nanocellulose is prepared by the acid hydrolysis of delignified cellulose from coconut midrib as depicted in Fig. 1. The high-resolution TEM images (Fig. 2a–c) indicate that the coconut midrib nanocellulose prepared has an average diameter of approximately 37 nm. Nanostructures seen in the TEM images showed a uniform morphology with a quasi-spherical shape and dimensional features. HRTEM images showed predominantly amorphous character with no lattice fringes discernible. AFM analysis of the coconut midrib nanocellulose was also carried out, and the results indicated the formation of nanoparticles with the average diameter ranging from 44 nm to 84 nm (Fig. S1, ESI†). Dynamic light scattering (DLS) was also used to obtain particle size distribution of the nanosized cellulose materials, which showed an average particle size of 63.17 nm (Fig. S2, ESI†). Zeta potential of the nanocellulose was also analysed using DLS, which showed negative zeta potential values ranging from −12 mV to −40 mV, indicating good stability in the dispersion (Fig. S3, ESI†). The SEM images of the coconut midrib nanocellulose clearly indicate the presence of nanofibers (Fig. S4, ESI†).

The presence of hydrogen bonds and van der Waals forces between adjacent molecules gives cellulose a characteristic crystalline structure, unlike hemicellulose and lignin, which are amorphous in nature.[29] The removal of lignin and hemicellulose increases the cellulose content, which in turn enhances the crystallinity of the fiber. The X-ray diffractogram (Fig. S5, ESI†) of the sample exhibited three distinct peaks near

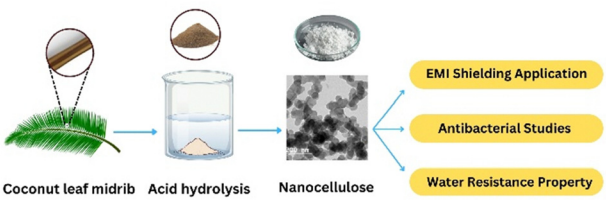

Fig. 1 Scheme of the preparation of coconut midrib nanocellulose.

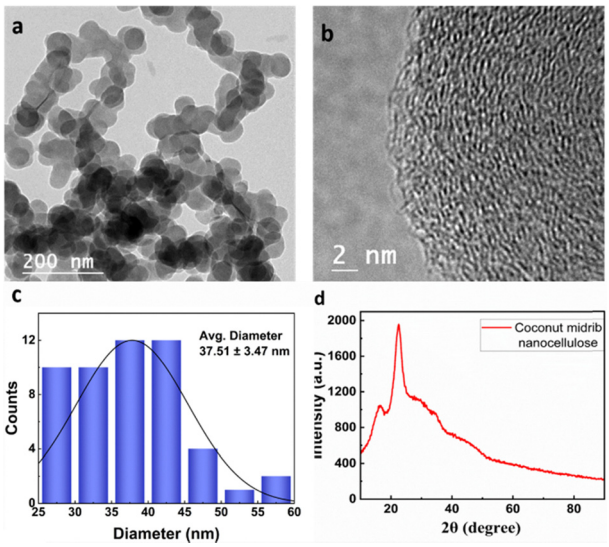

Fig. 2 (a) and (b) HRTEM images of the cellulose nanomaterial derived from coconut midrib; (c) histogram depicting the particle size distribution of the cellulose nanomaterial; (d) XRD pattern of the cellulose nanomaterial derived from coconut midrib.

2θ values of 16°, 22°, and 34° corresponding to the (110), (002), and (004) planes, which are characteristic crystalline peaks of cellulose I. The sample subjected to successive chemical treatments shows higher crystallinity compared to the untreated one. This is because the chemical treatments partially removed amorphous components such as hemicellulose and lignin. The crystalline structure of coconut midrib cellulose is similar to that found in other lignocellulosic fibers, such as pineapple leaf fiber, curaua, sisal, sugarcane bagasse, and others.[29] By comparing the diffractograms corresponding to various synthesis steps, it is observed that delignification and bleaching reactions did not cause any significant changes in the structure of cellulose, but rather removed the amorphous content. Amorphous hemicellulose and lignin can be effectively removed through alkali and bleaching treatments. The elimination of lignin and hemicellulose allows for tighter packing of cellulose chains, resulting in increased crystallinity.[30]

Comparison of the FTIR spectra (Fig. S6, ESI†) of raw coconut midrib, delignified fiber, fiber after first bleaching, and fiber after second bleaching clearly indicates the increase in the cellulose content. The spectra of the raw and delignified coconut midrib fiber are found to be similar. This suggests that the cellulose, hemicellulose, and lignin content of the samples did not undergo any significant chemical changes as a result of the sodium hydroxide delignification process. Both the raw and delignified samples exhibit peaks at 1461.33 cm^{-1}, which indicate the presence of the $-CH_2$ deformation vibration in the side chains. The absence of this peak in the spectrum of the bleached sample suggests that lignin has degraded. The peaks at 1637.64 cm^{-1} and 1505.54 cm^{-1} correspond to the stretching vibrations of C=O and the aromatic skeletal vibration of C=C in lignin, respectively.[31] These peaks were also absent in the spectra of the bleached sample, indicating that the bleaching procedure using hydrogen peroxide and sodium hydroxide could successfully remove lignin.

However, a characteristic peak at 1606 cm^{-1} with a notable intensity remained in the bleached samples, suggesting that the bleaching process did not fully eliminate the hemicellulose from the sample. Additionally, peaks were observed in the spectra of the raw, delignified, and bleached samples at 3327 cm^{-1} for –OH stretching vibration, 2918 cm^{-1} for C–H stretching vibration, 1430 cm^{-1} for $-CH_2$ and –OCH– plane bending vibrations, 1375 cm^{-1} for C–H deformation vibration, and 897 cm^{-1} for anomeric carbon (C1) vibration. These are all distinctive peaks of cellulose, demonstrating that highly pure cellulose was obtained.[31] It is very much evident from the FTIR analysis that the characteristic peaks of the bleached samples coincide with the reported FTIR peaks of cellulose, thus confirming the synthesis of pure cellulose from coconut midrib.

3.2 Characterization of cellulose nanopaper (CN)

CN, CN/CS, CN/PPy and CN/CS/PPy functionalized nanopapers were prepared in the desired dimensions and shapes (Fig. S7, ESI†). The FTIR spectra of pure CN derived out of coconut midrib nanocellulose and functionalized CN samples are shown in Fig. 3a. The peaks at 3334, 2917, 1650, 1427, 1164, 1107, and 890 cm^{-1} correspond to the characteristic peaks of cellulose I.[32] The peak at 1717 cm^{-1} corresponds to the C=O stretching from ester groups.[33] After the impregnation of chitosan to the pure CN, the peaks typical of chitosan appear in the FTIR spectrum. The prominent peaks at 3300 and 3353 cm^{-1} are attributed to N–H and O–H stretching, while the bands at 2923 and 2854 cm^{-1} correspond to symmetric and asymmetric CH stretching, respectively.[34]

The peak at 1650 cm^{-1} corresponds to the C=O stretching of amide I, while the peak at 1313 cm^{-1} corresponds to the C–N stretching of amide III. These peaks indicate the presence of residual N-acetyl groups. Additionally, the peaks at 1558 cm^{-1} and 1159 cm^{-1} correspond to the N–H bending of the primary amine and the asymmetric stretching of the C–O–C bridge, respectively.[35] The CH_2 bending and CH_3 symmetrical deformations are responsible for the bands at 1421 and 1370 cm^{-1}, respectively. The distinctive bands of polypyrrole are visible in the FTIR spectra of the sample polymerized with pyrrole. The pyrrole ring's C=C and C–N stretching vibrations are

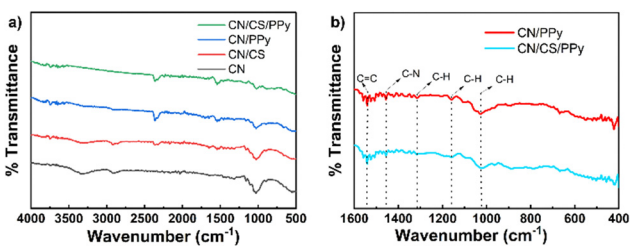

Fig. 3 (a) FTIR spectra of coconut midrib nanopaper (CN), coconut midrib nanopaper/chitosan (CN/CS), coconut midrib nanopaper/pyrrole (CN/PPy) and coconut midrib nanopaper/chitosan/pyrrole (CN/CS/PPy) films. (b) Comparison between spectra of coconut midrib nanopaper/pyrrole (CN/PPy) and coconut midrib nanopaper/chitosan/pyrrole (CN/CS/PPy).

responsible for the bands at 1541 and 1455 cm^{-1}, respectively.[36] The pyrrole ring's C–H in plane vibrations are responsible for the peaks at 1313, 1159, and 1030 cm^{-1}.[37] When we analysed Fig. 3b, we could find that the peaks in the spectrum of CN/CS/PPy are nearly equivalent to the peaks in CN/PPy, which indicates the formation of polypyrrole within the chitosan coating. The band at 1030 cm^{-1} of CN/PPy can be seen to change to a lower wavenumber, indicating that interactions exist between the chitosan and polypyrrole.[18]

SEM analysis revealed the morphology of the CN, CN/CS, CN/PPy and CN/CS/PPy samples (Fig. 4). The addition of chitosan makes the CN/CS surface smoother, and the cross-sectional analysis shows that denser interlayers as the voids between nanocellulose are filled with chitosan.[38] In the CN/PPy, numerous granular aggregates can be found, which denotes the presence of polypyrrole. After the introduction of polypyrrole, the CN/CS/PPy film becomes rougher than CN/CS, with visible polypyrrole granules observed in the image. However, the surface morphology is still smoother compared to CN/PPy. The interlayer of CN/CS/PPy expanded in comparison with CN/CS, but it is found to be denser when compared to CN/PPy. The tensile strength of the nanopaper samples was analysed and is given in Table S1 (ESI†). It is evident that the tensile strength is dependent on the composition of the films. These physical properties of CN/CS/PPy make it a promising material with higher electrical conductivity and better mechanical properties.

3.3 Wettability and water uptake

The water contact angle measurements and the water uptake ratio of the pure cellulose nanopaper (CN) and functionalized cellulose nanopaper samples (CN/CS, CN/PPy and CN/CS/PPy) were studied as depicted in Fig. 5. The CN film shows a comparatively lower contact angle of 48.70° and a high water uptake ratio of 96.21%. The CN films absorb water very quickly and get crimped. The high-water uptake ratio and the low contact angle of the CN film are attributed to the hydrophilic nature of the coconut midrib cellulose. The impregnation of chitosan to the pure film leads to drastic changes in wettability. The contact angle of CN/CS increased to 71.17°, and the water uptake ratio dropped to 78%. This is because of the high hydrophobicity and the relatively more complex structure of CN/CS films. The CN/CS strip got bent after the absorption of water, but it did not crimp as in the case of the CN film. The CN/PPy sample exhibited a higher contact angle of 80.85° and a reduced water uptake ratio of 70% compared to CN/CS. This change in water resistance measurements is attributed to the water resistance properties of pyrrole. The pyrrole layers hinder the penetration of water into the strip/film, retaining its shape even after immersion in water.[39] The CN/CS/PPy film exhibited a contact angle of 96.21° and an uptake ratio of 40%. As the contact angle of the film is above 90°, it proves that the surface of the film is hydrophobic. Also, when rinsed with water, the water droplets can be seen hardly retained on the surface of the film. Both these results confirm the hydrophobic nature of the CN/CS/PPy film. In the water uptake studies, the CN/CS, CN/PPy, and CN/CS/PPy strips preserved their original shape without any dissociation of CS or PPy, whereas the CN film nearly disintegrated into fragments. The water contact angle and the water uptake ratio of the films clearly illustrate the hydrophilic nature of the pure CNF film and the hydrophobic nature of the CN/CS/PPy film. The impregnation of chitosan and addition of pyrrole have made a drastic change in the nature of the film. The better water resistance properties of the functionalized film make it suitable for industrial and laboratory applications.

3.4 Antibacterial studies

Fig. 6 illustrates the antibacterial reduction studies of CN, CN/CS, CN/PPy and CN/CS/PPy samples against Gram-positive *Staphylococcus aureus* and Gram-negative *E. coli* (photographs of the inhibition zones of *Staphylococcus aureus* and *E. coli* bacteria are provided in Fig. S8 and S9, respectively, ESI†). The pure CN sample showed bacterial reductions of around 51.23% and 10.28% toward *Staphylococcus aureus* and *E. coli*, respectively, upon 30 minutes of contact. The disintegration of the CN film into fragments at the time of the vortexing process is the main reason for its bacterial reduction. The poor water

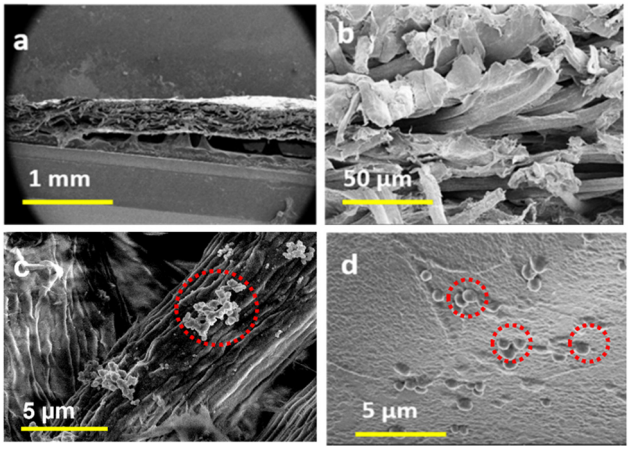

Fig. 4 SEM images of (a) coconut midrib nanopaper (CN), (b) coconut midrib nanopaper/chitosan (CN/CS), (c) coconut midrib nanopaper/pyrrole (CN/PPy) and (d) coconut midrib nanopaper/chitosan/pyrrole (CN/CS/PPy). The phases of polypyrrole are marked in (c) and (d).

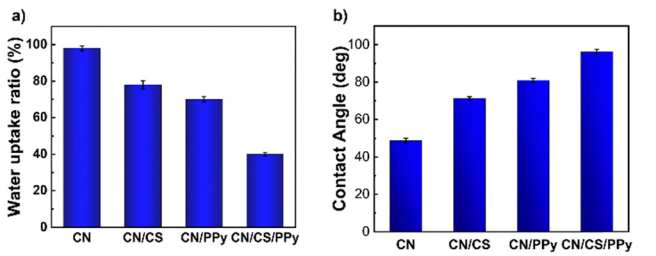

Fig. 5 (a) Graph of water uptake ratio of coconut midrib nanopaper (CN), coconut midrib nanopaper/chitosan (CN/CS), coconut midrib nanopaper/pyrrole (CN/PPy) and coconut midrib nanopaper/chitosan/pyrrole (CN/CS/PPy). (b) Contact angle measurements of coconut midrib nanopaper (CN), coconut midrib nanopaper/chitosan (CN/CS), coconut midrib nanopaper/pyrrole (CN/PPy) and coconut midrib nanopaper/chitosan/pyrrole (CN/CS/PPy).

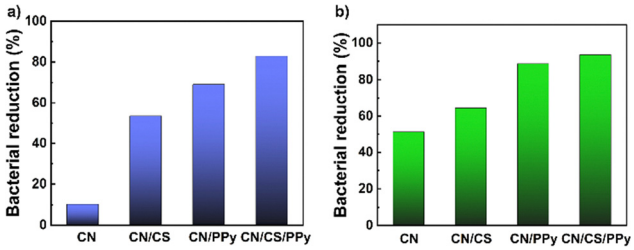

Fig. 6 (a) Graph of antibacterial reduction against Gram-negative bacteria. (b) Graph of antibacterial reduction against Gram-positive bacteria.

resistance properties of pure CN are the reason for the disintegration, and this allows bacteria to adhere to the porous surface of the fragments.[40] The impregnation of chitosan was the reason for the increased activity of the films against *Staphylococcus aureus* and *E. coli* with the reported bacterial reductions of 64.49% and 53.58%, respectively. The antibacterial property of chitosan is considered to be one of the reasons for the increased bacterial reduction. The electrostatic interaction between cationic chitosan and the negatively charged bacterial cell membrane damages the membrane, leading to the leakage of cellular contents and cell death.[41] The CN/PPy film shows significant antibacterial activity towards *Staphylococcus aureus* and *E. coli* with bacterial reductions of 88.69% and 69.14%, respectively. The positive charge associated with the polypyrrole is another reason for the bacterial reduction of the films.[42] The CN/CS/PPy film exhibited enhanced activity towards *Staphylococcus aureus* and *E. coli* with bacterial reductions of 93.47% and 82.79%, respectively. The enhanced antibacterial activity of the functionalized film is due to the presence of chitosan and polypyrrole. Along with the excellent antibacterial properties, the mechanical strength and water resistance properties make the functionalized CNF film a potential material for biomedical applications.

3.5 Electromagnetic interference shielding

We studied the EMI shielding application of the CN/CS/PPy, and the results are presented in Fig. 7 and Fig. S11 (ESI†). The CN/CS is taken as a control sample, and its shielding effectiveness is found to be nearly zero. This is mostly because of the nature of CN/CS, which allows the electromagnetic wave to pass through the CN/CS film matrix easily. The CN/PPy film displays

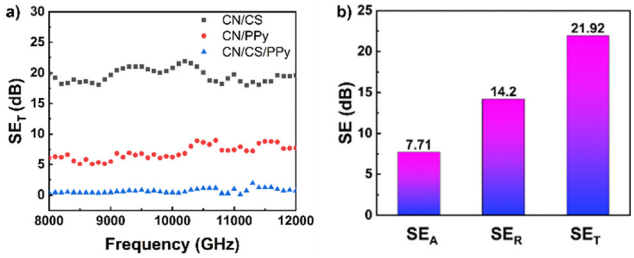

Fig. 7 (a) SE_T *vs.* frequency (GH_z) graph of coconut midrib nanopaper/chitosan/pyrrole (CN/CS/PPy); (b) SE (dB) *vs.* SE_R, SE_A, and SE_T graph of coconut midrib nanopaper/chitosan/pyrrole (CN/CS/PPy).

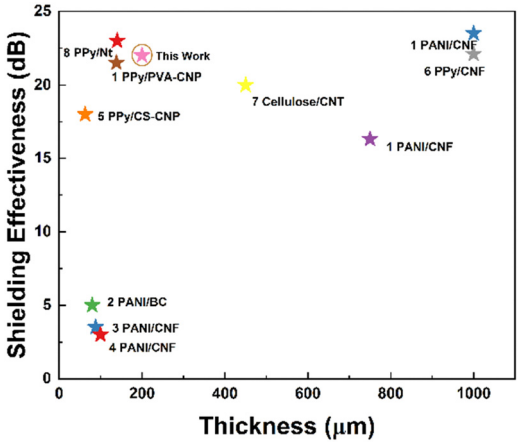

Fig. 8 Comparison of EMI shielding performance of the conducting polymer and cellulose based composite films from the literature.[33,45–51]

a shielding effectiveness of 6 dB at 10 GHz. The CN/CS/PPy film exhibits a high shielding effectiveness of about 21.92 dB at 10 GHz at a thickness of 200 μm, which apparently hinders 99% of the electromagnetic radiation. The shielding effectiveness is a result of the conductivity of the CNP/CS/PPy film (1.06×10^{-4} S cm^{-1}, as shown in Fig. S10, ESI†) and the heterostructure of the CN/CS/PPy film. The SE_T, SE_A, and SE_R values of the CN/CS/PPy film at 10 GHz are compared in order to understand the shielding mechanism involved in it. Fig. 6b illustrates that the SE_R contribution to the SE_T is significantly greater than that of SE_A, which can be attributed to the heterostructure of the CN/CS/PPy film.[43] The chitosan and polypyrrole in the CN/CS/PPy film are the reason for its conductivity, and CNFs act as insulating nanofillers, thus making them unique heterostructures. The heterostructures in the film are responsible for the multiple reflections in the matrix, leading to microwave absorption. When incident microwaves encounter the CN/CS/PPy heterostructure, they are reflected by the highly conductive layer formed by chitosan and polypyrrole. The remaining part of the incident microwave is reflected at the interfaces in the film present between non-conductive CNFs and conductive chitosan/polypyrrole. The heterostructures formed inside the functionalized film play a crucial role in deciding the shielding mechanism and its effectiveness.[44] When the EMI shielding effectiveness values of composites with cellulose and conducting polymers are compared, CN/CS/PPy showed a better shielding effectiveness in relation to its thickness, as depicted in Fig. 8. With the shielding performance, mechanic strength, lightweight, excellent flexibility, and an easy, low-cost method for preparation, the obtained CN/CS/PPy has promising potential as a sustainable EMI shielding material.

4. Conclusions

In this work, we have prepared nanocellulose from coconut midrib using optimized pre-treatment steps and an acid hydrolysis process. To the best of our knowledge, this is the first report of the preparation of nanocellulose from coconut

midrib. The FTIR analysis revealed that the delignification and bleaching procedures did remove most of the hemicellulose and lignin from the coconut midrib fiber. XRD analysis showed the increase in crystallinity through the various stages of synthesis of coconut midrib nanocellulose. The HRTEM and DLS analyses confirmed the synthesis of coconut midrib nanocellulose. This work presents a novel approach for efficiently utilizing coconut midrib as a potential feedstock for producing cellulose nanofibrils. We prepared cellulose nanopaper from cellulose derived from coconut midrib and demonstrated a simple approach to functionalize the cellulose nanopaper for achieving multifunctional applications. Chitosan was impregnated to the cellulose nanopaper followed by the introduction of polypyrrole through *in situ* polymerization. The CN/CS/PPy film exhibited excellent water-resistant properties. The CN/CS/PPy film showed good antibacterial activity toward Gram-negative and Gram-positive bacteria, with a bacterial reduction of 93.47% for *Staphylococcus aureus* and a bacterial reduction of 89.79% for *E. coli*. The CN/CS/PPy film with its good electrical conductivity and high shielding effectiveness, around 21.92 dB at 10 GHz at a thickness of 200 μm, can be considered as a potential option for large scale production of the electromagnetic shielding material.

Author contributions

VTP conceptualized the work from planning to execution. JJ performed all the experiments, compiled the results, drew the figures (including the graphical abstract), and wrote the manuscript. Both VTP and JJ were involved in the internal revision of the manuscript.

Data availability

The data supporting this article have been included as part of the ESI.†.

Conflicts of interest

There are no conflicts to declare.

Acknowledgements

Joshua Jose acknowledges CHRIST University for the research fellowship. Vinod T. P. is thankful to the Vision Group on Science and Technology, Government of Karnataka, for the K-FIST-L1 grant (GRD No. 1143). The authors acknowledge Dr Partha Kumbhakar, Assistant Professor, Department of Physics and Electronics, CHRIST University, for the tensile strength measurements.

Notes and references

1 M. Bexell and K. Jönsson, Responsibility and the United Nations' Sustainable Development Goals, *Forum Dev. Stud.*, 2017, **44**(1), 13–29. Available from: https://www.tandfonline.com/doi/full/10.1080/08039410.2016.1252424.

2 M. Chandra Manna, M. M. Rahman, R. Naidu, A. Sahu, S. Bhattacharjya and R. H. Wanjari, *et al.*, Bio-Waste Management in Subtropical Soils of India, *Adv. Agron.*, 2018, 87–148. Available from: https://linkinghub.elsevier.com/retrieve/pii/S0065211318300622.

3 P. H. Brunner and H. Rechberger, Waste to energy – key element for sustainable waste management, *Waste Manage.*, 2015, **37**, 3–12. Available from: https://linkinghub.elsevier.com/retrieve/pii/S0956053X14000543.

4 M. Duque-Acevedo, L. J. Belmonte-Ureña, N. Yakovleva and F. Camacho-Ferre, Analysis of the Circular Economic Production Models and Their Approach in Agriculture and Agricultural Waste Biomass Management, *Int. J. Environ. Res. Public Health*, 2020, **17**(24), 9549. Available from: https://www.mdpi.com/1660-4601/17/24/9549.

5 L. J. Pham, Coconut (Cocos nucifera), *Industrial Oil Crops*, 2016, pp. 231–242.

6 M. Gopal, A. Gupta, K. Shahul Hameed, N. Sathyaseelan, T. H. Khadeejath Rajeela and G. V. Thomas, Biochars produced from coconut palm biomass residues can aid regenerative agriculture by improving soil properties and plant yield in humid tropics, *Biochar*, 2020, **2**(2), 211–226.

7 G. V. Thomas, V. Krishnakumar, R. Dhanapal and D. V. S. Reddy, Agro-management practices for sustainable coconut production, *Coconut Palm (Cocos nucifera L.)–Research and Development Perspectives*, 2019, pp. 227–322.

8 S. K. Malhotra, H. P. Maheswarappa, V. Selvamani and P. Chowdappa, Diagnosis and management of soil fertility constraints in coconut (Cocos nucifera): A review, *Indian J. Agric. Sci.*, 2017, **87**(6), 711–726.

9 I. M. Rajendra, I. N. S. Winaya, A. Ghurri and I. K. G. Wirawan, Pyrolysis study of coconut leaf's biomass using thermogravimetric analysis, *IOP Conf. Ser.: Mater. Sci. Eng.*, 2019, **539**(1), 012017.

10 Y. Zhao, A. Tagami, G. Dobele, M. E. Lindström and O. Sevastyanova, The impact of lignin structural diversity on performance of cellulose nanofiber (CNF)-starch composite films, *Polymers*, 2019, **11**(3), 538.

11 P. S. Bakshi, D. Selvakumar, K. Kadirvelu and N. S. Kumar, Chitosan as an environment friendly biomaterial – a review on recent modifications and applications, *Int. J. Biol. Macromol.*, 2020, **150**, 1072–1083. Available from: https://linkinghub.elsevier.com/retrieve/pii/S0141813018357933.

12 M. Wu, P. Sukyai, D. Lv, F. Zhang, P. Wang and C. Liu, *et al.*, Water and humidity-induced shape memory cellulose nanopaper with quick response, excellent wet strength and folding resistance, *Chem. Eng. J.*, 2020, **392**, 123673. Available from: https://linkinghub.elsevier.com/retrieve/pii/S1385894719330888.

13 N. D. Sanandiya, A. R. Pai, S. Seyedin, F. Tang, S. Thomas and F. Xie, Chitosan-based electroconductive inks without chemical reaction for cost-effective and versatile 3D printing for electromagnetic interference (EMI) shielding and strain-sensing applications, *Carbohydr. Polym.*, 2024, **337**, 122161. Available from: https://linkinghub.elsevier.com/retrieve/pii/S0144861724003874.

14 W. Wang, Q. Meng, Q. Li, J. Liu, M. Zhou and Z. Jin, *et al.*, Chitosan Derivatives and Their Application in Biomedicine, *Int. J. Mol. Sci.*, 2020, **21**(2), 487. Available from: https://www.mdpi.com/1422-0067/21/2/487.

15 A. Nautiyal, M. Qiao, T. Ren, T. S. Huang, X. Zhang and J. Cook, *et al.*, High-performance Engineered Conducting Polymer Film towards Antimicrobial/Anticorrosion Applications, *Eng. Sci.*, 2018, 70–78. Available from: https://www.espublisher.com/journals/articledetails/34/.

16 A. Nautiyal, M. Qiao, J. E. Cook, X. Zhang and T. S. Huang, High performance polypyrrole coating for corrosion protection and biocidal applications, *Appl. Surf. Sci.*, 2018, **427**, 922–930. Available from: https://linkinghub.elsevier.com/retrieve/pii/S0169433217324285.

17 M. Zhang, A. Nautiyal, H. Du, J. Li, Z. Liu and X. Zhang, *et al.*, Polypyrrole film based flexible supercapacitor: mechanistic insight into influence of acid dopants on electrochemical performance, *Electrochim. Acta*, 2020, **357**, 136877. Available from: https://linkinghub.elsevier.com/retrieve/pii/S0013468620312706.

18 G. Ruhi, O. P. Modi and S. K. Dhawan, Chitosan-polypyrrole-SiO2 composite coatings with advanced anticorrosive properties, *Synth. Met.*, 2015, **200**, 24–39. Available from: https://linkinghub.elsevier.com/retrieve/pii/S0379677914004536.

19 A. R. Pai, Y. Lu, S. Joseph, N. M. Santhosh, R. Degl'Innocenti and H. Lin, *et al.*, Ultra-broadband shielding of cellulose nanofiber commingled biocarbon functional constructs: A paradigm shift towards sustainable terahertz absorbers, *Chem. Eng. J.*, 2023, **467**, 143213. Available from: https://linkinghub.elsevier.com/retrieve/pii/S1385894723019447.

20 Y. Zhao, C. Xu, C. Xing, X. Shi, L. M. Matuana and H. Zhou, *et al.*, Fabrication and characteristics of cellulose nanofibril films from coconut palm petiole prepared by different mechanical processing, *Ind. Crops Prod.*, 2015, **65**, 96–101. Available from: https://linkinghub.elsevier.com/retrieve/pii/S0926669014007651.

21 S. H. Hassan, T. S. Velayutham, Y. W. Chen and H. V. Lee, TEMPO-oxidized nanocellulose films derived from coconut residues: Physicochemical, mechanical and electrical properties, *Int. J. Biol. Macromol.*, 2021, **180**, 392–402. Available from: https://linkinghub.elsevier.com/retrieve/pii/S0141813021005833.

22 C. Xu, S. Zhu, C. Xing, D. Li, N. Zhu and H. Zhou, Isolation and Properties of Cellulose Nanofibrils from Coconut Palm Petioles by Different Mechanical Process, *PLoS One*, 2015, **10**(4), e0122123. Available from: https://dx.plos.org/10.1371/journal.pone.0122123.

23 L. U. S. Faria, B. J. S. Pacheco, G. C. Oliveira and J. L. Silva, Production of cellulose nanocrystals from pineapple crown fibers through alkaline pretreatment and acid hydrolysis under different conditions, *J. Mater. Res. Technol.*, 2020, **9**(6), 12346–12353. Available from: https://linkinghub.elsevier.com/retrieve/pii/S2238785420317014.

24 W. J. Orts, J. Shey, S. H. Imam, G. M. Glenn, M. E. Guttman and J. F. Revol, Application of Cellulose Microfibrils in Polymer Nanocomposites, *J. Polym. Environ.*, 2005, **13**(4), 301–306. Available from: https://link.springer.com/10.1007/s10924-005-5514-3.

25 L. Hu, H. Du, C. Liu, Y. Zhang, G. Yu and X. Zhang, *et al.*, Comparative Evaluation of the Efficient Conversion of Corn Husk Filament and Corn Husk Powder to Valuable Materials via a Sustainable and Clean Biorefinery Process, *ACS Sustainable Chem. Eng.*, 2019, **7**(1), 1327–1336. Available from: https://pubs.acs.org/doi/10.1021/acssuschemeng.8b05017.

26 H. Du, M. Parit, K. Liu, M. Zhang, Z. Jiang and T. S. Huang, *et al.*, Multifunctional Cellulose Nanopaper with Superior Water-Resistant, Conductive, and Antibacterial Properties Functionalized with Chitosan and Polypyrrole, *ACS Appl. Mater. Interfaces*, 2021, **13**(27), 32115–32125. Available from: https://pubs.acs.org/doi/10.1021/acsami.1c06647.

27 M. Peng and F. Qin, Clarification of basic concepts for electromagnetic interference shielding effectiveness, *J. Appl. Phys.*, 2021, **130**(22), 225108.

28 Y. Chen, L. Pang, Y. Li, H. Luo, G. Duan and C. Mei, *et al.*, Ultra-thin and highly flexible cellulose nanofiber/silver nanowire conductive paper for effective electromagnetic interference shielding, *Composites, Part A*, 2020, **135**, 105960.

29 K. S. Prado and M. A. S. Spinacé, Isolation and characterization of cellulose nanocrystals from pineapple crown waste and their potential uses, *Int. J. Biol. Macromol.*, 2019, **122**, 410–416. Available from: https://linkinghub.elsevier.com/retrieve/pii/S014181301833976X.

30 Y. Song, J. Zhang, X. Zhang and T. Tan, The correlation between cellulose allomorphs (I and II) and conversion after removal of hemicellulose and lignin of lignocellulose, *Bioresour. Technol.*, 2015, **193**, 164–170.

31 Y. Song, J. Zhang, X. Zhang and T. Tan, The correlation between cellulose allomorphs (I and II) and conversion after removal of hemicellulose and lignin of lignocellulose, *Bioresour. Technol.*, 2015, **193**, 164–170. Available from: https://linkinghub.elsevier.com/retrieve/pii/S0960852415008755.

32 K. Liu, H. Du, T. Zheng, H. Liu, M. Zhang and R. Zhang, *et al.*, Recent advances in cellulose and its derivatives for oilfield applications, *Carbohydr. Polym.*, 2021, **259**, 117740.

33 H. Du, M. Parit, M. Wu, X. Che, Y. Wang and M. Zhang, *et al.*, Sustainable valorization of paper mill sludge into cellulose nanofibrils and cellulose nanopaper, *J. Hazard. Mater.*, 2020, **400**, 123106.

34 C. Branca, G. D'Angelo, C. Crupi, K. Khouzami, S. Rifici and G. Ruello, *et al.*, Role of the OH and NH vibrational groups in polysaccharide-nanocomposite interactions: A FTIR-ATR study on chitosan and chitosan/clay films, *Polymer*, 2016, **99**, 614–622.

35 S. Yasmeen, M. Kabiraz, B. Saha, M. Qadir, M. Gafur and S. Masum, Chromium(VI) Ions Removal from Tannery Effluent using Chitosan-Microcrystalline Cellulose Composite as Adsorbent, *Int. Res. J. Pure Appl. Chem.*, 2016, **10**(4), 1–14.

36 M. Zhang, A. Nautiyal, H. Du, J. Li, Z. Liu and X. Zhang, *et al.*, Polypyrrole film based flexible supercapacitor: mechanistic insight into influence of acid dopants on electrochemical performance, *Electrochim. Acta*, 2020, **357**, 136877.

37 X. Zhang, X. Wu, C. Lu and Z. Zhou, Dialysis-free and in situ doping synthesis of polypyrrole@cellulose nanowhiskers

nanohybrid for preparation of conductive nanocomposites with enhanced properties. ACS Sustainable, *Chem. Eng.*, 2015, **3**(4), 675–682.

38 H. Du, M. Parit, K. Liu, M. Zhang, Z. Jiang and T. S. Huang, *et al.*, Multifunctional Cellulose Nanopaper with Superior Water-Resistant, Conductive, and Antibacterial Properties Functionalized with Chitosan and Polypyrrole, *ACS Appl. Mater. Interfaces*, 2021, **13**(27), 32115–32125.

39 M. Parit, H. Du, X. Zhang, C. Prather, M. Adams and Z. Jiang, Polypyrrole and cellulose nanofiber based composite films with improved physical and electrical properties for electromagnetic shielding applications, *Carbohydr. Polym.*, 2020, **240**, 116304.

40 W. Ma, L. Li, X. Xiao, H. Du, X. Ren and X. Zhang, *et al.*, Construction of Chlorine Labeled ZnO–Chitosan Loaded Cellulose Nanofibrils Film with Quick Antibacterial Performance and Prominent UV Stability, *Macromol. Mater. Eng.*, 2020, **305**(8), 200028.

41 Z. Cao and Y. Sun, N-Halamine-based chitosan: Preparation, characterization, and antimicrobial function, *J. Biomed. Mater. Res., Part A*, 2008, **85**(1), 99–107.

42 F. A. G. da Silva Júnior, S. A. Vieira, S. de A. Botton, M. M. da Costa and H. P. de Oliveira, Antibacterial activity of polypyrrole-based nanocomposites: a mini-review, *Polimeros*, 2020, **30**(4), e2020048. Available from: **https://www.scielo.br/scielo.php?script=sci_arttext&pid=S0104-14282020000400501&tlng=en**.

43 Y. Zhang, M. Qiu, Y. Yu, B. Wen and L. Cheng, A Novel Polyaniline-Coated Bagasse Fiber Composite with Core–Shell Heterostructure Provides Effective Electromagnetic Shielding Performance, *ACS Appl. Mater. Interfaces*, 2017, **9**(1), 809–818. Available from: **https://pubs.acs.org/doi/10.1021/acsami.6b11989**.

44 T. W. Lee, S. E. Lee and Y. G. Jeong, Highly Effective Electromagnetic Interference Shielding Materials based on Silver Nanowire/Cellulose Papers, *ACS Appl. Mater. Interfaces*, 2016, **8**(20), 13123–13132. Available from: **https://pubs.acs.org/doi/10.1021/acsami.6b02218**.

45 M. Parit, H. Du, X. Zhang, C. Prather, M. Adams and Z. Jiang, Polypyrrole and cellulose nanofiber based composite films with improved physical and electrical properties for electromagnetic shielding applications, *Carbohydr. Polym.*, 2020, **240**, 116304. Available from: **https://linkinghub.elsevier.com/retrieve/pii/S0144861720304781**.

46 J. A. Marins, B. G. Soares, M. Fraga, D. Müller and G. M. O. Barra, Self-supported bacterial cellulose polyaniline conducting membrane as electromagnetic interference shielding material: effect of the oxidizing agent, *Cellulose*, 2014, **21**(3), 1409–1418. Available from: **https://link.springer.com/10.1007/s10570-014-0191-9**.

47 T. Omura, C. H. Chan, M. Wakisaka and H. Nishida, Organic Thin Paper of Cellulose Nanofiber/Polyaniline Doped with (±)-10-Camphorsulfonic Acid Nanohybrid and Its Application to Electromagnetic Shielding, *ACS Omega*, 2019, **4**(5), 9446–9452. Available from: **https://pubs.acs.org/doi/10.1021/acsomega.9b00708**.

48 P. Gahlout and V. Choudhary, Microwave shielding behaviour of polypyrrole impregnated fabrics, *Composites, Part B*, 2019, **175**, 107093. Available from: **https://linkinghub.elsevier.com/retrieve/pii/S1359836818343609**.

49 H. D. Huang, C. Y. Liu, D. Zhou, X. Jiang, G. J. Zhong and D. X. Yan, *et al.*, Cellulose composite aerogel for highly efficient electromagnetic interference shielding, *J. Mater. Chem. A*, 2015, **3**(9), 4983–4991. Available from: **https://xlink.rsc.org/?DOI=C4TA05998K**.

50 D. A. Gopakumar, A. R. Pai, Y. B. Pottathara, D. Pasquini, L. Carlos de Morais and M. Luke, *et al.*, Cellulose Nanofiber-Based Polyaniline Flexible Papers as Sustainable Microwave Absorbers in the X-Band, *ACS Appl. Mater. Interfaces*, 2018, **10**(23), 20032–20043. Available from: **https://pubs.acs.org/doi/10.1021/acsami.8b04549**.

51 T. Lapka, J. Vilčáková, D. Kopecký, J. Prokeš, M. Dendisová and R. Moučka, *et al.*, Flexible, ultrathin and light films from one-dimensional nanostructures of polypyrrole and cellulose nanofibers for high performance electromagnetic interference shielding, *Carbohydr. Polym.*, 2023, **309**, 120662. Available from: **https://linkinghub.elsevier.com/retrieve/pii/S0144861723001261**.